JOURNAL OF MATERIALS SCIENCE 26 (1991) 5383–5395

Mechanical testing of plasma-sprayed ceramic coatings on metal substrates: interfacial fracture toughness and tensile bond strength

M. J. FILIAGGI, R. M. PILLIAR
Centre for Biomaterials, and The Department of Metallurgy and Materials Science, University of Toronto, Toronto, Ontario, Canada M5S 1A4

Plasma-sprayed ceramic coatings applied to metal components have uses in many diverse fields, including aerospace, electronics and, more recently, biomaterials. In all such applications success of the component relies on adequate bonding between the ceramic coating and metal substrate. In this study, a convenient and reliable test method to assess the fracture toughness of this metal/ceramic interface was developed by modifying an existing homogeneous short-bar configuration. Additionally, conventional tensile adhesive bond strength testing was conducted. For the alumina-coated Ti–6Al–4V model system studied, an interface toughness value of 1.84 ± 0.20 MPa $m^{1/2}$ was obtained. An interfacial tensile bond strength of 13.6 ± 2.9 MPa was also measured for this system. Further refinement of this modified short bar technique taking into account experimental compliance behaviour and potential complex or mixed-mode stress intensities is needed to confirm these preliminary toughness values, which nevertheless offer a potentially more sensitive means of monitoring the mechanical integrity of this metal/ceramic interface.

1. Introduction

Plasma-sprayed ceramic coatings have applications in many diverse areas, including aerospace and electronics. When applied to metal components, these coatings can greatly enhance performance and the range of applications of these metals by functioning, for example, as thermal barrier or wear-resistant coatings [1–3]. This surface modification technique has also attracted much interest in the biomaterials field, where functional improvements in dental and orthopaedic implant devices have been sought. The discovery of bioceramic materials such as hydroxyapatite (HA) that can actively interact with skeletal tissues has led to further exploitation of the plasma-spraying process. As coatings, these so-called bioactive ceramics offer the potential for long-term, biological fixation of coated metallic implants to bone through chemical bonding of the coating with the surrounding bone tissue. However, success of these plasma-sprayed HA-coated implant systems relies on maintaining the integrity of the metal/ceramic interface during implant loading.

To date, no adequate standardized test method exists for determining the fracture resistance and adhesive bond strength of plasma-sprayed ceramic coatings on metal. The tensile bond test is perhaps the most attractive and frequently used [4] of the currently available test methods owing to its overall simplicity and the existence of test standards. Here, the load is applied perpendicular to the interface and the failure load per cross-sectional area is measured. Generally for these tests, a support fixture is attached by means of an epoxy adhesive to the coated substrate so that the tensile force can be applied. Several variations of this tensile bond test exist [5], although standardized tests such as ASTM C633 and DIN 50160, have been specifically developed to test the adhesive/cohesive bond strength of these plasma-sprayed coatings.

In theory, these tensile bond tests are relatively simple to perform and serve as good sources of qualitative information. However, the usefulness of this test as a quantitative tool is questionable due to some serious limitations and concerns, not the least of which is the frequently erratic nature of the test results [6, 7]. This scatter may arise from true material differences (defects, pores and inclusions) from one specimen to another leading to premature failure, or from variations associated with the test method [7]. In addition, the data are dependent upon the particular test method and specimen size employed, hence the need for standardized testing [8, 9]. Typical tensile bond strength values reported for plasma-sprayed ceramic coatings on metal range from 6–40 MPa [2]. Other bond strength evaluation techniques exist, but they tend to be used much less frequently for plasma-sprayed coatings and are more or less qualitative in nature [5, 8, 10–13].

The objectives of our study were to develop a convenient and reliable test method to assess the fracture toughness of the metal/ceramic interface formed on plasma-sprayed metal substrates, as well as to conduct further studies on the use of interfacial

0022–2461/91 $03.00 + .12 © *1991 Chapman & Hall*

tensile bond testing. Although the intended application was directed to the study of a specific bioactive ceramic coating (hydroxyapatite) on titanium alloy substrates [14], we used a model system (plasma-sprayed Al_2O_3 on Ti–6Al–4V) to develop the test method. The choice of a plasma-sprayed alumina coating was based on availability of alumina powders and on the vast experience reported in the literature and in industry with producing these coatings. It should be noted that the use of alumina-coated metallic biomaterials has been suggested in the past and thus represents additionally a potential practical biomaterials system.

The use of interfacial fracture toughness to assess ceramic to metal bonding in these plasma-sprayed systems is not new. Modified double cantilever beam (DCB) tests have been reported for the determination of the critical strain energy release rate, G_{Ic}, for different plasma-sprayed ceramic-coated metal substrate systems [15–21]. Overall, these studies revealed a problematic feature of this modified DCB method, namely the systematic dependence of G_{Ic} (or K_{Ic}) on crack length. Additionally, crack instability at short crack lengths attributed to both specimen geometry and loading system compliance was experienced [20]. Double torsion testing of these ceramic–metal systems has also been attempted [21]. Unfortunately, few specifics regarding test methodology were provided, and thus a proper analysis of this study could not be performed. Ferber and Brown [22] and Ferber [23] undertook a fracture mechanics study of plasma-sprayed alumina-coated Ti–6Al–4V and 316L stainless steel in physiological environments, focusing in particular on subcritical crack growth and stress corrosion. Although the primary intent of their investigation was to generate V–K curves (crack velocity versus stress intensity), K_{Ic} determinations also were made using pre-cracked cylindrical four-point bend specimens.

The test that we have studied and that is described herein relies on the use of a specimen design involving a chevron or V-shaped notch. This geometry was originally created to allow for initiation and arrest of a crack in brittle materials, which are inherently difficult to pre-crack, by relying on high initial stress intensity at the notch tip and a limited amount of stored elastic energy at the moment of fracture initiation [24–26]. Increased tri-axial constraint of the crack is also possible due to the thin chevron slots [25, 27]; thus, smaller specimens are required to maintain plane-strain conditions for a valid toughness measurement. In addition, fracture toughness measurements are relatively straightforward. As the crack grows, the stress intensity factor, K, passes through a minimum at the maximum load, which is therefore used in K determinations.

Recently, the use of chevron-notched short-bar and short-rod configurations has been described by Barker [28, 29], leading to the development of an ASTM specification (ASTM B771) employing this test method. From the short bar/rod (SB/R) technique, K_{Ic} is calculated from the maximum load achieved and the minimum stress intensity factor coefficient or stress intensity normalization factor, A_m, using the equation

$$K_{IcSB/R} = \frac{P_c}{B^{3/2}} A_m \quad (1)$$

Here, the critical stress intensity factor is designated by $K_{IcSB/R}$ to emphasize the fundamental differences between this method of fracture toughness determination and that dictated in ASTM E399. A complete derivation of the short bar/rod fracture toughness equation for calculating the critical stress intensity factor is described by Barker [28, 29].

The potential for using the chevron-notched short bar/rod specimens to determine the fracture toughness at the interface of dissimilar materials has been demonstrated by Melcholsky and Barker [30]. Specifically, they examined two ceramic–metal systems with negligible differences in thermal expansion coefficients using a composite specimen in which one-half of the specimen was metal and the other ceramic. To utilize published compliance calibrations derived for homogeneous specimens, the authors altered the dimensions of one-half of the standard specimen using a theoretical analysis based on elementary beam theory. Although the bond toughness test could now be treated as a standard K_{IcSB} test, the authors emphasized that G_{Ic} was, in fact, a more appropriate measure of fracture toughness of the interface, because their K_{Ic} values depended on whether the metal or ceramic was to have the dimensions of the standard half-specimen. Although a promising approach to interface fracture toughness evaluation, no follow-ups to this study have been reported.

In the study reported herein, the interfacial fracture toughness of plasma-sprayed alumina-coated Ti–6Al–4V substrates is determined using a novel composite short-bar configuration. Additionally, the mechanical integrity of this system is examined using conventional tensile bond testing.

2. Methods

2.1. Materials

The Ti–6Al–4V substrate material for this study was supplied in the mill-annealed condition with a certified chemical composition satisfying ASTM specification F136-84 for surgical-grade extra-low interstitial (ELI) Ti–6Al–4V. Pertinent information regarding the starting alumina powders can be found in Table I.

2.2. Plasma-spraying parameters

Table I lists some important plasma-spraying parameters for the alumina coating study. For this system, plasma spraying was done by the Plasma Technology Research Centre, University of Sherbrooke (US; Sherbrooke, Quebec), with some preliminary assistance being provided by a local company (Jay-Em Ceramics, Brampton, Ontario).

2.3. Interfacial fracture toughness testing

2.3.1. Specimen design and assembly

The design of the composite short-bar specimen was based primarily on the standardized homogeneous

TABLE I Plasma-spraying parameters

Spray powder	Source, designation	AMDRY no. 180
	Chemical composition	min. 99% alumina
	Particle size distribution	15–55 μm
Surface preparation	Surface roughening	60-grit alumina, 25 p.s.i. gritblasting pressure, 90°
	Surface cleaning	ultrasonically in acetone
Coating deposition	Primary plasma gas	argon
	Secondary plasma gas	nitrogen
	Carrier gas	argon
	Powder feed rate	0.7 kg h^{-1}
	Power	40 kW
	Environment	Low pressure: 550 mm Hg
	Stand-off distance	7 cm
	Specimen holder configuration and motion	wheel; rotational
	Relative gun motion	translational along the axis of rotation
	Substrate/coating surface temperature control	Water and air jets at the surface; air barrier to divert hot plasma gases

short-bar specimen configuration as outlined in ASTM B771 for the testing of cemented carbides. For this study, it was necessary to create short-bar specimen halves, with one-half providing the surface for coating and the other acting, with the use of an adhesive, as the mating half to complete the specimen (Fig. 1a). The Ti–6Al–4V specimen halves were machined from bar stock and possessed standard width and breadth dimensions of 19.05 and 12.70 mm, respectively, and nominal thicknesses or half-heights of 5.33 mm.

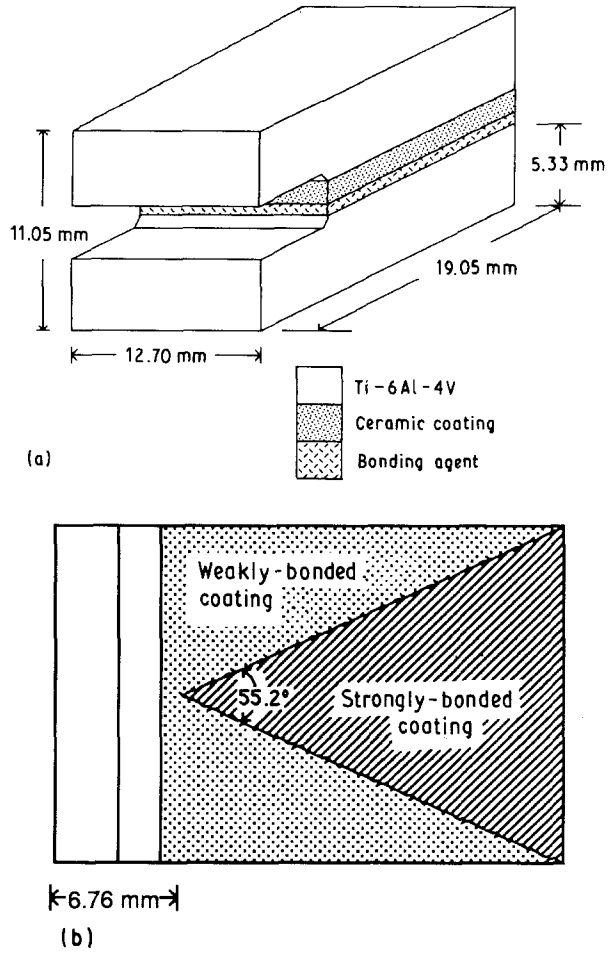

Figure 1 (a) Schematic drawing of the modified composite short-bar specimen; (b) top view of a coated short-bar half showing regions of weakly and strongly bonded coating.

The surfaces of these specimen halves were then prepared for coating in the following manner. The entire surface was either sandblasted (60-grit silica, 80 p.s.i. (10^3 p.s.i. = 6.89 N mm^{-2}), 90°, 30 s) to produce a lightly roughened surface, wet ground using a series of successively finer grit SiC metallographic papers to a 600-grit surface finish, or diamond polished from the 600 grit surface down to a 1 μm diamond finish. After cleaning the specimens ultrasonically in acetone, a gritblasting-resistant polymer-based tape, cut with the aid of a template, was placed over the prepared surface to expose a chevron-shaped region beginning at a desired distance, a_0, of 6.76 mm from the front face and having a standard angle, θ, of 55.2°, as outlined in ASTM B771 for a straight-slotted chevron. a_0 and θ values of the masked samples were measured using a Mitutoyo toolmakers microscope (Model TM-201). With the tape protecting the prepared surface outside of the chevron, the surfaces of the specimen halves were then gritblasted (see Table I) to produce a highly roughened chevron region. Following a second ultrasonic cleaning in acetone, the halves were coated using the deposition parameters indicated in Table I to a coating thickness of approximately 250–300 μm. When possible, specimens having different surface preparations were placed in the same holding jigs or wheels for plasma spraying to eliminate as a variable in the study intrinsic differences between plasma-spraying runs. The end result of this selective surface treatment on relative coating adhesion, shown schematically in Fig. 1b, is a strongly bonded coating in the chevron region surrounded by a weakly bonded coating in the "outer" region.

Prior to specimen assembly, coating thicknesses were determined by measuring the "half-heights" of the specimens in several locations before and after coating using a rounded-tip digital micrometer head with a flat base. A final ultrasonic cleaning in acetone was also performed to remove excess moisture absorbed by the coatings and to improve the adhesive/ceramic bond.

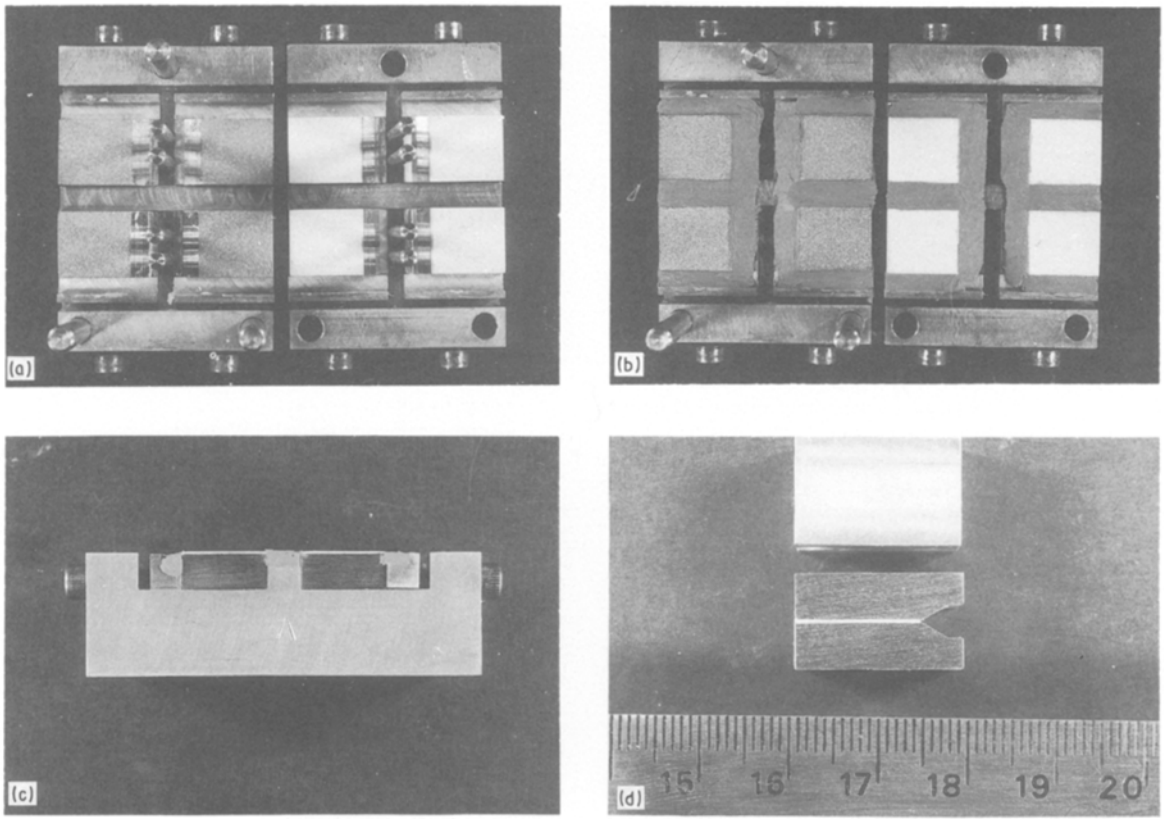

Figure 2 Assembly of the short-bar halves using a multiple customized aligning jig: (a) coated specimen halves with their mating, uncoated halves; (b) application of the modelling clay to protect exposed metal surfaces and to prevent adhesive uptake by the coatings from the edge; (c) side view of the coated halves in the assembly jig, with modelling clay up to the coating surface; (d) the assembled short-bar specimen.

Coated specimens were then mated to roughened but uncoated Ti–6Al–4V halves having identical pre-coating dimensions using a multiple customized aligning jig (Fig. 2). A-2 epoxy resin adhesive with activator W (Armstrong Products, Warsaw, IN) in a 1.5:1 volume ratio was used with a room-temperature cure to bond the specimen halves. To prevent adhesive penetration by capillary action into the coating from the sides, and thus potential bonding with metal at the metal/ceramic interface, modelling clay was moulded up to the coating surface (see Fig. 2).

For all assembled specimens, excess bonding agent forced out from between the halves was removed using a scalpel prior to final curing. All specimens were also assembled with the coating facing downwards to minimize adhesive penetration into the coatings. The overall height or thickness of the composite specimen achieved with these aligning jigs (Fig. 2d) corresponded approximately to the value of 11.05 mm dictated for the standardized homogeneous short-bar specimens.

2.3.2. Testing protocol

Testing of the modified short-bar specimens was based on procedures outlined in ASTM B771 for short bar/rod testing of cemented carbides, with some simplifications. The gripping mechanism recommended in the standard was adopted for this study. Adaptors then allowed for stress transfer from these grips to the load cell through a universal joint and to the crosshead above and below the specimen, respectively (Fig. 3). Provisions were made for monitoring mouth opening displacements by modifying a standard extensometer (Instron model G51-16MA) to suit the specimen configuration and loading. Specimens were tested

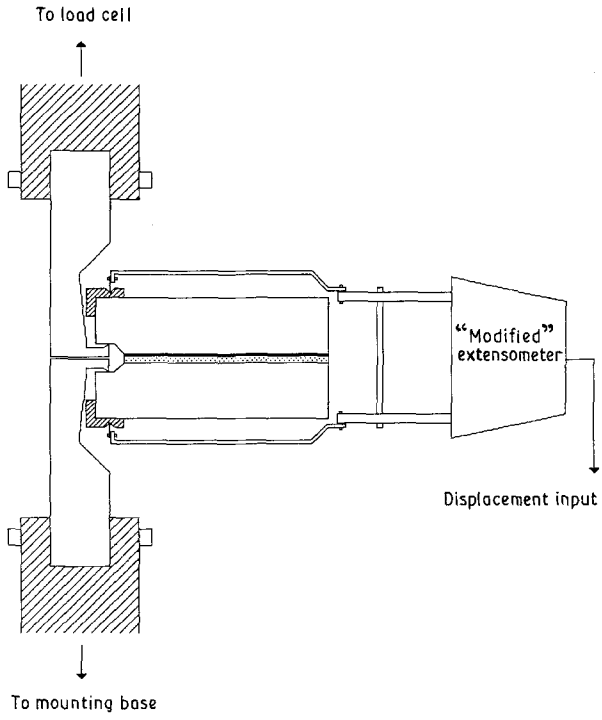

Figure 3 Schematic drawing of the test set-up for the modified short-bar specimens showing the gripping mechanism and adaptors, and the positioning of the extensometer around the specimen.

to failure using an Instron universal testing machine (Model TT-CM) under Mode I loading conditions at a crosshead speed of 0.05 cm min^{-1} and load–displacement curves recorded. Generally, the extensometer was not sufficiently stable to provide reasonable displacement measurements. In these cases, only the necessary peak load measurement was made.

2.3.3. Fracture toughness/K_{IcSB} calculations

The critical stress intensity factor (K_{IcSB}) was determined from the relation for a homogeneous short bar, assuming linear elastic behaviour

$$K_{IcSB} = \frac{A_m P_c}{B^{3/2}} C_c \quad (2)$$

where B is the specimen breadth (12.70 mm), A_m is the dimensionless calibration constant, equal to 22 for homogeneous short-bar specimens with this standard scaled geometry, and P_c is the maximum load achieved in the experiment. C_c, defined in ASTM B771 as a specimen configuration correction factor, allows for some corrections to the calculated K_{IcSB} values due to out-of-tolerance specimen dimensions. When possible, corrections for out-of-tolerance a_0 and θ values were made using the procedures outlined in this standard. For values deviating from the standard by more than three times the tolerance, it was necessary to use an extrapolation/interpolation technique presented by Barker [31] to determine A_m values for slightly "non-standard" specimen configurations. This correction was based on experimental compliance versus crack length measurements on the standard "family" and on specimens which purposely differed from this family with respect to a_0 and θ.

2.4. Tensile bond testing

Tensile bond testing in this study was conducted using the specifications outlined in ASTM C633 for adhesive or cohesive strength testing of flame-sprayed coatings, with a few notable exceptions. Here, tensile specimens with less than the minimum standardized diameter of 23 mm were used in order to allow for use of available bar stock. In addition, coating thicknesses were less than the conservative lower limit of 380 μm set by the standard. Note, however, that this standard was developed for the testing of coatings deposited by one of several flame-spraying techniques, including oxyacetylene flame spraying, a thermal spraying method known to produce less dense (i.e. more porous) coatings than those obtained by plasma flame spraying.

2.4.1. Specimen assembly

To produce the tensile specimen shown schematically in Fig. 4, tensile specimen halves, approximately 2.54 cm long, were first cut from 12.57 mm diameter bar stock and machined to produce parallel faces. 6.35 mm holes centred approximately 9.5 mm from the bottom face were then drilled perpendicular to the longitudinal axis to allow the specimens to be placed in the load cell adaptors using a "pin and clevis" arrangement. The surfaces to be coated were subsequently prepared according to the surface treatments employed in the corresponding modified short-bar specimens. As with the alumina short-bar specimens, tensile specimen halves were cleaned ultrasonically in acetone prior to coating.

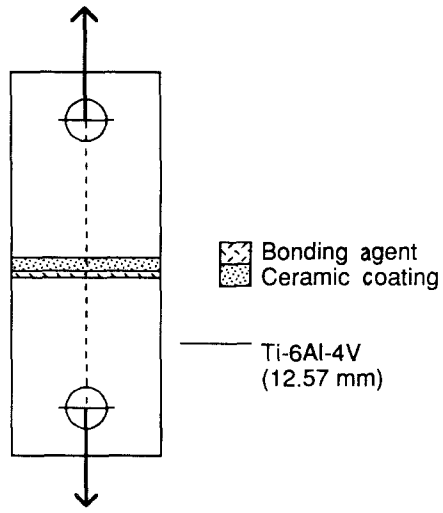

Figure 4 Schematic drawing of the tensile bond test specimen.

Subsequent to assembly, several layers of Teflon tape were wrapped around the specimen circumference, encompassing the metal/ceramic interface and a majority of the coating. The role of the Teflon tape was similar to the modelling clay employed in the short-bar assembly, namely, to prevent adhesive uptake into the coating from the edge by capillary action, which may alter the adhesive or cohesive strength of the coating. Coated specimens were then mated to roughened, but uncoated, halves using the bonding agent and a multiple aligning jig (Fig. 5). Low pressure, created either manually or with the use of a dead weight, enabled consistently thin glue lines to be produced. As with the short-bar specimens, halves were mated with the coating facing downwards in order to minimize adhesive penetration into the coating during curing. In addition, excess adhesive was removed prior to complete curing.

2.4.2. Testing protocol

Tensile specimens were tested using an Instron universal testing machine with adaptors designed to grip and transfer loads to the specimens. Additionally, a universal joint from the load cell was employed as a self-aligning mechanism in order to minimize shear forces at this interface or within the coating. Samples were pulled in tension at 0.1 cm min^{-1} crosshead speed, and the maximum load value was recorded. Bond strengths were determined by dividing the peak load recorded during the test by the cross-sectional area of the specimen. For samples in which mixed-mode failure was evident (e.g. failure at the metal/ceramic interface and within the bulk coating), a valid bond strength determination was not possible.

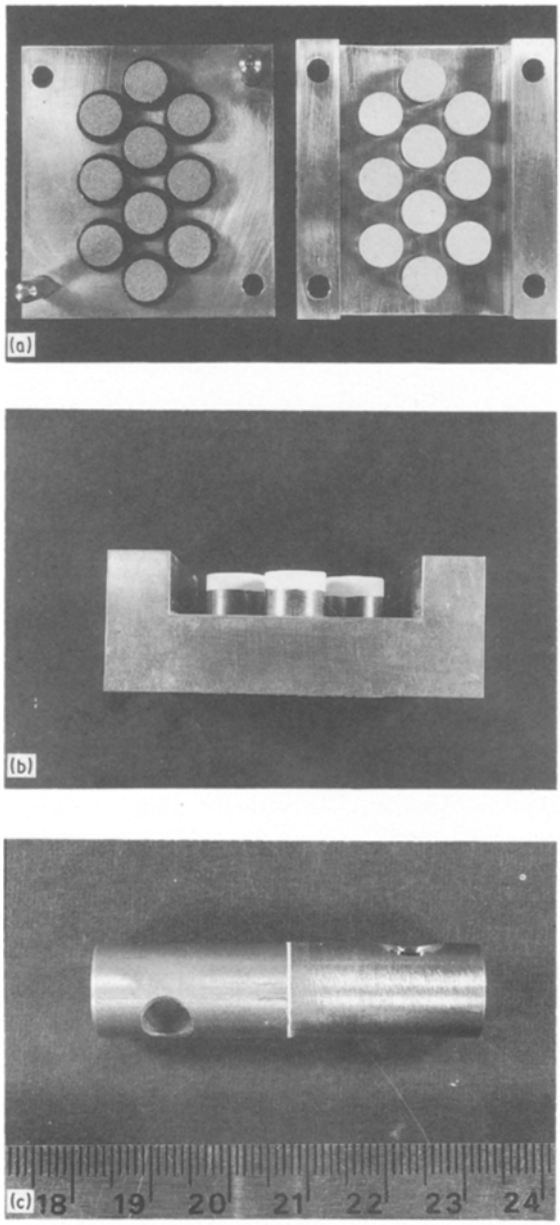

Figure 5 Assembly of the tensile specimen using a multiple aligning jig: (a) coated specimen halves with the mating, uncoated halves; (b) side view of the coated halves, with Teflon tape up to the coating surface; (c) the assembled specimen.

2.5. Failure analysis

The fracture surfaces of both tensile and short-bar test specimens were qualitatively inspected to determine the mode of failure. For this study, the failure mode designations in Table II were employed. Additionally, representative specimens from each test group and specimens for which the mode of failure was not clearly evident were examined by scanning electron microscopy and energy dispersive X-ray analysis.

Arithmetic means and standard deviations from these means were determined for tensile bond strength and fracture toughness test groups having similar surface preparations and modes of failure. In addition, a one-way analysis of variance (ANOVA) of the data was performed.

TABLE II Failure mode designations

Designation	Failure Location
M/C	Metal/ceramic interface
C (I)	In the ceramic coating, at or very near the interface
C	Cohesively within the ceramic coating
A/C	Adhesive/ceramic interface
A	Cohesively within the adhesive
M/A	Metal/adhesive interface

2.6. Additional/supplementary characterization techniques

2.6.1. Coating morphology and porosity

General coating morphology was assessed by SEM, as was the presence of any defect structures, including porosity, inclusions, and microcracks. When possible, both planar and cross-sectional samples were examined. From alumina free-standing coatings, porosity was measured by mercury intrusion using an Autoscan-60 Porosimeter (Model SP-20LV) interfaced with a microcomputer.

2.6.2. Surface roughness measurements

For all of the surface treatments employed in this study, including 600-grit and diamond polished surfaces, surface roughnesses of the substrate were measured using a 7100 Series Surf-Analyser System (Gould, Cleveland). All measurements were made in microinches (μin; 1 μin = 2.54×10^{-6} cm) and represented arithmetic average (AA) roughness values. In addition, these surfaces were examined using the SEM to discern general topographical features.

3. Results

3.1. General characterization

3.1.1. Coating morphology and porosity

General morphology of the alumina coatings can be discerned from the scanning electron micrographs in Fig. 6. All coatings demonstrated to some extent the characteristic lamellar nature of plasma-sprayed coatings. Examination of planar sections of the alumina coatings parallel to the interface revealed the plate-like structure which produces this layered appearance.

The coatings also exhibited some degree of porosity. This porosity either took the form of "smooth" pores circular in cross-section and emanating from the plate-like features, or irregular (and in some cases channel-like) pores discernible between individual plates or layers. From mercury intrusion data, 5% porosity with a mean pore size of 9×10^{-2} μm was determined. This is in general agreement with previously reported porosity data for plasma-sprayed alumina coatings [32, 33]. Note, however, that measurements using this technique are not wholly accurate, as they do not account for closed pores or "bottle-neck" pores, which the mercury cannot infiltrate, or the compressibility of the mercury and the sample. The measurement is further dependent on coating thickness, because closed porosity tends to increase with coating thickness [34].

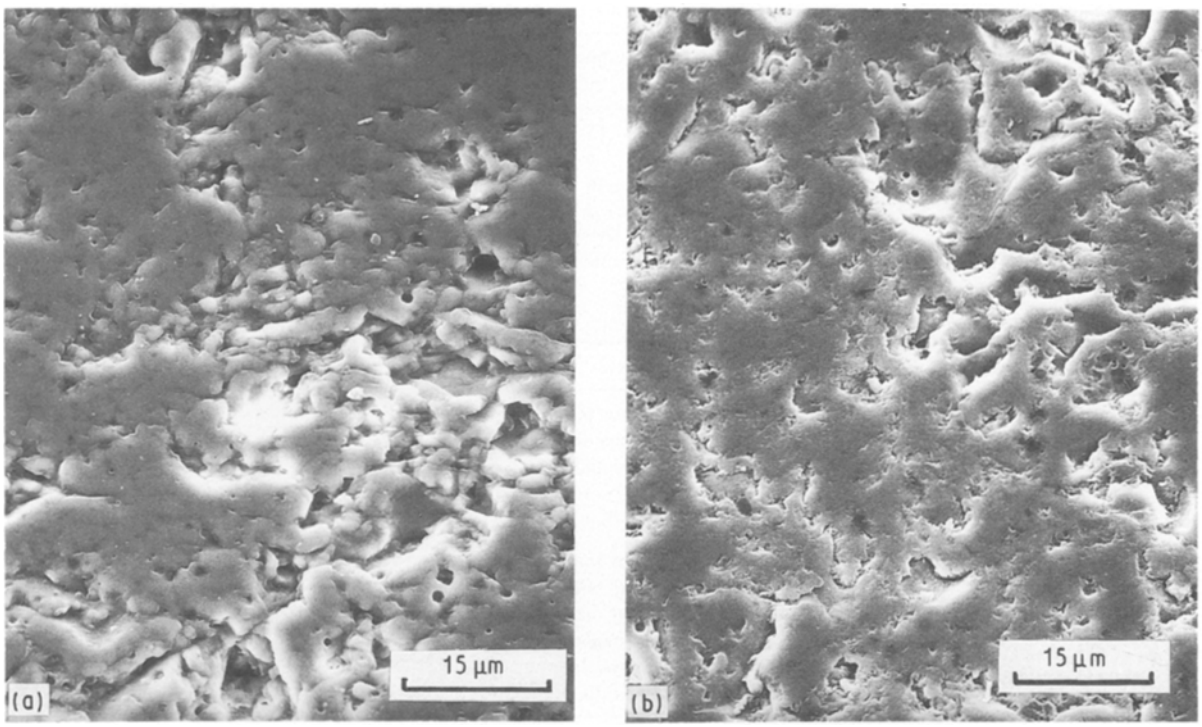

Figure 6 (a) Alumina coating cross-section; (b) planar section revealing the plate-like structure of the splats.

3.1.2. Substrate surface roughness

To analyse the effect of substrate surface preparation on mechanical test data, surface roughnesses were determined from "representative" gritblasted surfaces and surfaces employed in the region outside of the chevron in the modified short-bar specimen. These values are shown in Table III.

3.2. Data analysis

Fracture toughness data are reported in Table IV for several batches of US-coated samples. For batch 3 (US-3) samples, the primary focus of this study, a complete analysis of outer region variations on the measured fracture toughness data was possible. Other batch runs were not, however, amenable to extensive analysis and statistical treatment due to the preliminary nature of the study (US-1), or inadequate sample populations (US-2) arising from unanticipated changes in plasma-spraying parameters and subsequent unexpected post-assembly failure behaviour. Nevertheless, results for modified short-bar specimens with a sandblasted or 600-grit finish outer region are reported for US-1 and US-2, respectively, as they allow for some qualitative assessment of the sensitivity of the short-bar technique to changes in plasma-spraying parameters. Note that in Table IV, K_{IcSB} values are listed along with "corrected" K_{IcSB} values which take into account out-of-tolerance dimensions, specifically with regards to a_0 and θ. In all cases, these corrections had little if any effect on mean fracture toughness values and standard deviations, indicating the relative insensitivity of this test method to small changes in a_0 or θ.

Difficulties in seating the extensometer around the specimen in a stable manner resulted in unreliable load versus mouth opening displacement curves for some of these short-bar tests. When the extensometer

TABLE III Surface roughness values[a]

Surface[b]	Roughness (μin)	(μm)
Gritblasted	120–140	(3.0–3.6)
Sandblasted	25–30	(0.6–0.8)
600-grit	7–10	(0.2–0.3)
Diamond	5–7	(0.1–0.3)

[a] Arithmetical average (AA).
[b] Surfaces from prepared blanks.

TABLE IV K_{IcSB} determinations – alumina coated Ti–6Al–4V

Designation	Coating thickness (μm)	Outer region preparation	Number of samples	K_{IcSB} (MPa $m^{1/2}$)	"Corrected" K_{IcSB} (MPa $m^{1/2}$)	Failure mode (chevron – outer)
US-3	250 ± 20	sandblasted	5	2.61 ± 0.25	2.56 ± 0.27	C (I)–M/C
US-3	260 ± 15	600-grit	4	1.91 ± 0.30	1.89 ± 0.29	C (I)–M/C
US-3	250 ± 20	diamond	3	1.88 ± 0.21	1.84 ± 0.20	C (I)–M/C
US-1	250 ± 20	sandblasted	6	3.51 ± 0.07	3.51 ± 0.07	C (I) + C–M/C + C(I)
US-2	220 ± 15	600-grit	2	2.89 ± 0.42	2.85 ± 0.39	C(I)–M/C

TABLE V Tensile bond strength data – alumina-coated Ti–6Al–4V

Designation	Surface	Coating thickness (μm)	Number of samples	Bond strength (MPa)	Failure mode
US-3[a]	gritblasted	330 ± 60	15	13.6 ± 2.9	C (I)
US-3[a]	sandblasted	300 ± 50	5	7.2 ± 1.8	C (I)
US-3[a]	600-grit	285 ± 50	6	9.1 ± 2.7	~ M/C + C (I)
US-3[a]	diamond	260 ± 70	4	5.2 ± 1.3	~ M/C + C (I)

[a] Thickness variations no greater than 25 μm on any one sample; average coating thicknesses vary greatly sample to sample within a group.

TABLE VI Statistical analysis (ANOVA)–alumina

Test	Group	Subgroup pairs	Analysis	p
Short bar	US-3	sandblast versus 600-grit	S	< 0.0167
		sandblast versus diamond	S	< 0.0167
		600-grit versus diamond	NS	> 0.0167
	600-grit outer	US-2 versus US-3	S	< 0.05
	Sandblasted outer	US-1 versus US-3	S	< 0.0167
Tensile	US-3	gritblast versus sandblast	S	< 0.0083
		gritblast versus 600-grit	S	< 0.0083
		gritblast versus diamond	S	< 0.0083
		sandblast versus 600-grit	NS	> 0.0083
		sandblast versus diamond	NS	> 0.0083
		600-grit versus diamond	NS[a]	> 0.0083

[a] Statistically significant difference at 98.33% when outer region preparation examined as group.

was stable, however, a typical load–displacement curve such as the one shown in Fig. 7 was produced. Generally, peak loads were reached at approximately 20 μm mouth opening displacement.

The corresponding tensile bond strength data for alumina-coated Ti–6Al–4V are presented in Table V. Included in this table are bond strength values achieved with the primary gritblasted surfaces found in the chevron regions of the short bar samples, as well as values obtained with surface preparations equivalent to the "outer" regions in the same samples. The "well-bonded" coatings generally exhibited lower tensile bond strengths than have previously been reported for this system [35, 36]. (Note that no useful tensile data are available for US-1 and US-2 due to the reasons stated above.)

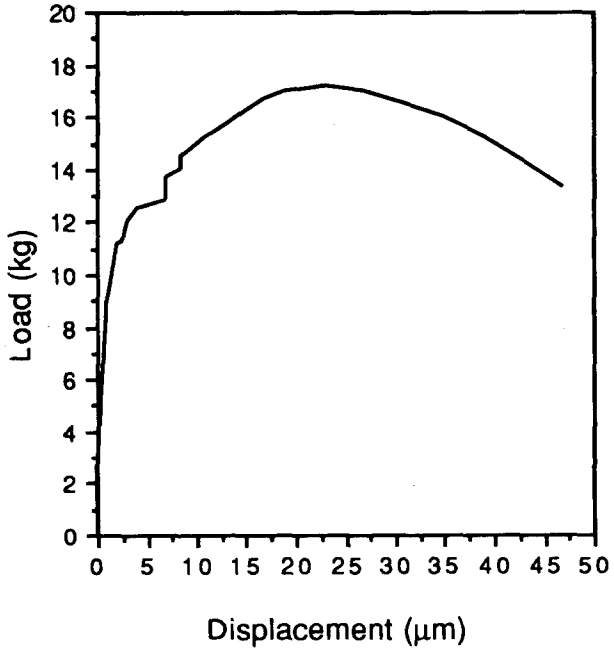

Figure 7 Load–displacement curve obtained when the extensometer behaved in a stable manner, showing mouth opening displacement of 20–25 μm at the peak load.

To allow for viable statistical comparisons between test groups, particularly owing to the smaller sample sizes for the short-bar evaluations, one-way analysis of variance (ANOVA) was performed on selected sample groups, with differences discerned between corresponding subgroup pairs making up the base group. Results of this statistical analysis are shown in Table VI for the fracture toughness and tensile results. In general, statistically significant differences in raw data were demonstrated between nearly all of the short-bar subgroup pairs considered, the one exception being US-3 specimens with either a 600-grit or diamond-polished surface finish in the "outer" region.

Not surprisingly, tensile data generated from the US-coated samples possessing a gritblasted surface were shown to be statistically different from data obtained with samples from the same batch but with the smoother, "outer" surface preparations. Despite decreases in surface roughness from a sandblasted surface to a diamond-polished finish, no discernible differences in tensile bond strength were obtained between the groups possessing the outer surface preparations. However, when the gritblasted US specimens were not included in an analysis of these three groups, statistically significant differences at slightly less stringent probability levels did appear between specimens having the 600-grit and diamond-polished substrate surface finishes.

3.3. Failure analysis

While relatively clean failure at the metal/ceramic interface was evident in the outer regions of the US-coated short-bar specimens, more alumina was retained in the gritblasted grooves of the chevron region and on the tensile specimen surfaces (Figs 8 and 9),

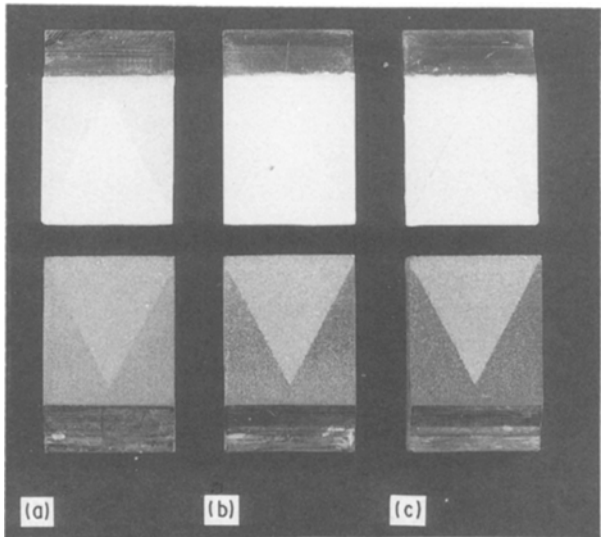

Figure 8 Alumina-coated short-bar specimens after failure, showing the failed metal surface (bottom) and the removed coating (top) for different surface preparations in the region outside of the chevron: (a) sandblasted; (b) 600-grit; (c) diamond-polished.

prompting the creation of failure designation C(I) to indicate cohesive-like failure in the coating at or very near the metal/ceramic interface. Examination of the failed metal surfaces at high magnification revealed the presence of significant alumina splats around, and in some cases over the top of, asperities on the metal surface (Fig. 10). In the region surrounding the chevron, isolated retention of alumina "islands" was detected, even in the case of the diamond-polished surface shown in Fig. 10b. To all intents and purposes, however, failure occurred in this region at the metal/ceramic interface. The surfaces of the corresponding mating halves are shown in Fig. 10c and d.

The failure pattern described above was repeated in other US-coated short-bar specimens, although failure in the first batch (US-1) was marked by reproducibly

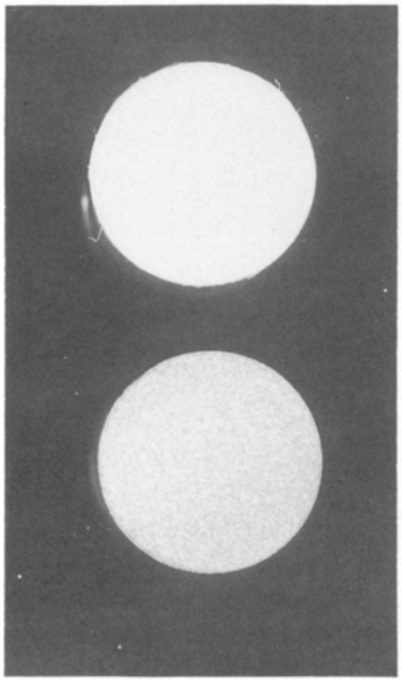

Figure 9 Alumina-coated tensile specimen after failure, showing the failed metal surface (bottom) and the removed coating (top).

increased retention of alumina in both the chevron and outer regions. Failure of the tensile specimens (US-3), specifically those with the outer region preparation, tended to be less consistent over the whole surface, partly due to misalignment of the wheel holder with respect to the plasma gun during the coating operation [37].

4. Discussion

4.1. K_{IcSB} measurements and the weakly bonded outer region

A unique aspect of the modified short-bar test developed in the study was the weakly bonded coating in the outer region surrounding the gritblasted chevron zone. This weakly bonded coating was included in the overall design of the specimen for two reasons: firstly, it provided a relatively simple and reliable means of protecting the exposed metal surface from the adhesive or bonding agent; secondly, it was expected to encourage crack initiation and subsequent propagation at the metal/ceramic interface. An implicit assumption in preliminary fracture toughness studies with these alumina-coated systems was that the contribution of this "outer" region to toughness determinations was negligible. To discern if the weakly bonded zone affected peak load values obtained at the critical crack length, a_c, corresponding to the position of stable-to-unstable crack growth, the surface roughness in this region was progressively reduced from that of a sandblasted surface to a diamond-polished surface in order to reduce bonding effectively in this region. As the results in Table IV and the corresponding statistical (ANOVA) analysis indicate, toughness values were reduced significantly in going from a sandblasted outer region to one with a 600-grit SiC finish. However, no further reduction was achieved with a subsequent diamond-polished finish, suggesting that the fracture toughness values were no longer sensitive to bonding in this "outer" region.

Of potential concern, however, is the high bond strengths possible with either the 600-grit or diamond-polished finishes as demonstrated in the tensile bond tests. That the decrease in roughness in going from the sandblasted to the diamond-polished surface (cf. Table III) failed to produce a corresponding statistically significant decrease in bond strength is unexpected and not easily explained. Arguably, small sample sizes, particularly for a tensile test, were used in the analysis; this fact, in conjunction with scatter that was significant compared to the short bar testing, may have rendered the tensile test insensitive to this variable change. Still, this does not explain the exceedingly high bond strengths obtained with the 600-grit finish. Thus, further investigation with these polished surfaces is warranted. Unfortunately, finding additional ways to reduce this bond strength to negligible values (i.e. $\sim$ 0 MPa) was complicated by the specific coating deposition parameters. For example, applying a salt "film" to the surface that could be subsequently dissolved after plasma spraying, as is sometimes done to obtain free-standing (i.e. detached) coatings, was not possible due to the use of air-atomized water jets in the surface cooling system.

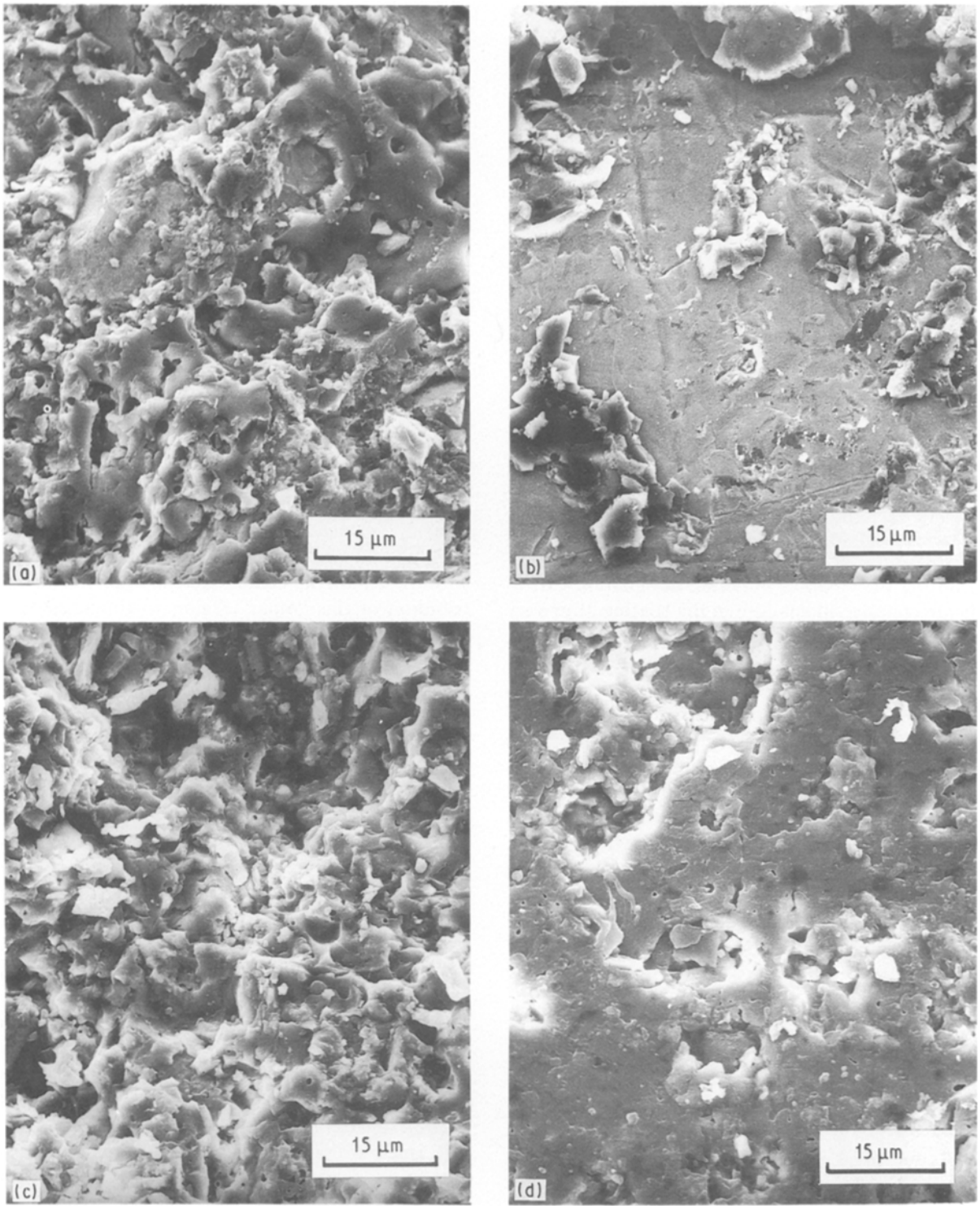

Figure 10 Fractographic analysis of the failed short bar specimen: (a) the failed metal surface revealing significant retention of alumina on the surface; (b) the failed metal surface in the "outer" region, showing some alumina remnants even on a diamond-polished surface. The corresponding mating halves with the removed alumina coating in (c) the chevron region and (d) "outer" region, revealing more extensive splat spreading with the smooth metal surface.

The "base-line" interfacial fracture toughness values measured from specimens having the 600-grit or diamond-polished outer surfaces are higher than the value of 1.2 ± 0.2 MPa $m^{1/2}$ reported by Ferber and Brown [22] for this system. Significant differences in plasma-spraying parameters (e.g. much lower gun power and stand-off distance in the earlier study) undoubtedly account for some of this discrepancy. Additionally, the pre-cracked four-point bend specimens used in their study had a tendency to fail cohesively as well as adhesively. Their toughness values, therefore, may have been skewed towards the toughness of porous alumina. Also, it is noteworthy that the fracture toughness data obtained in the present study did exhibit less scatter compared to the corresponding tensile bond strength data, potentially making the former more amenable to parametric studies.

4.2. Modified short-bar sensitivity

The primary objective of our study was the development of this modified short-bar test. To discern the

sensitivity of fracture toughness values measured by this technique to changes in coating conditions, a controlled parameter study involving spraying distance was also attempted. Unfortunately, this study was unsuccessful due to unanticipated dilatation of the sample holder used during plasma spraying, resulting in a loss of specimens and thus an inadequate sample population. However, some observations involving the three coating batches can be made. A comparison can be drawn, for example, between short-bar specimens from US-2 and US-3 specimens having the 600-grit finish in the "outer" region. Despite the smaller sample size, the results from these groups were found to be significantly different ($p < 0.05$), with US-2 demonstrating a higher interfacial fracture toughness (Table IV). This decrease in toughness from batch 2 to batch 3 can potentially be traced to an effective reduction in cooling in the latter coating session as a result of asymmetric positioning of the coating wheel relative to the spray gun and associated cooling jets, and alterations in the design and positioning of the rods making up part of the cooling jet system [37].

A similar argument for inadequate cooling can be made when comparing US-3 short-bar specimens with their counterparts in batch 1 (US-1). Again, the above changes to batch 3 apply here. Additionally, an air tube was added to the final two batch runs to purge the spraying chamber of water vapour which had accumulated at the top of the chamber. The extra stress on the system's compressor resulted in a reduction in the pressure of the cooling air jet, thus further reducing the effective cooling of the specimen surface [37]. Overall, then, residual stresses at the interface were likely more prominent for US-3 short-bar specimens compared to the preceding batch runs, and this is reflected in reduced fracture toughness at the metal/ceramic interface.

4.3. Modified short-bar compliance and K_{IcSB} measurements

An important assumption made in the calculation of K_{IcSB} values in this study was that the modified short bar specimens could be assigned an A_m value corresponding to a homogeneous specimen of the same scaled geometry. Because A_m, the minimum stress intensity factor coefficient, is derived from compliance (c) versus crack length (a) data, specifically dc/da [28, 29, 31], the implication was that the modified and homogeneous short bars displayed the same compliance behaviour. To a first approximation, this is the case.

Compliance is a function of geometry and materials properties, specifically modulus. For modified short-bar specimens lacking a weakly bonded coating in the region outside of the chevron, a situation equivalent to the homogeneous short bar is obtained with respect to geometry. It is only necessary, therefore, to determine the effect that the ceramic coating and bonding agent have on the modulus of the specimen as a whole. By treating the short bar specimen as two cantilever beams, one can use elementary beam theory to approximate the influence of these additional materials on the modulus of a specimen that, from a per cent thickness aspect, is essentially Ti–6Al–4V. Here, an asymmetric situation is created if one assumes crack propagation along the metal/ceramic interface. For this analysis, the two extreme cases were examined by assuming that either the adhesive or ceramic accounted for the "non-Ti–6Al–4V" thickness. Not surprisingly, this second component added little to the flexural modulus of the specimen "half" in either case, with the composite half effectively acting like a Ti–6Al–4V half with half-height (H) of 5.33 mm. Note in this study, however, that the A_m value used in K_{IcSB} assumed a homogeneous short bar having a total height ($2H$) of 11.05 mm to correspond to the standard scaled geometry. Using an expression for Y_m^* ($\propto A_m$) derived by Munz *et al.* [27] for specimens having initial crack length-to-width ratios between 0.2 and 0.5, and width-to-half height ratios between 3 and 4, one finds that specimens having half-heights of 5.33 mm instead of the standard half-height of 5.53 mm, alter Y_m^* by only about 3%. Thus, the compliance behaviour of this modified short-bar specimen can be approximated by that of the homogeneous short-bar specimen with the standard scaled geometry.

The above argument can also be applied to modified specimens having a weakly bonded coating in the "outer" region. However, the presence of this region does alter the geometry, and therefore the compliance at a specified crack length in another way. Because dc/da rather than c is needed in the determination of A_m, and because this modified short-bar geometry with the "outer" region can be modelled as a short bar with a straight-through notch, a direct reference can be made to the compliance study by Munz *et al.* [27]. In their study, it was assumed initially that dc/da for a chevron notch was the same as for a straight-through notch. Subsequently, Y_m^* values (related to A_m by a constant) based on this assumption were found to be within 3.5% of the Y_m^* values derived from experimental compliance testing of chevron-notched short bars. (Agreement is even better ($\sim 1\%$) for short bars having the initial crack length to specimen width ratio used in our study.) Thus, at the critical crack length, a_c, the "outer" region appears to make very little contribution to the compliance behaviour of the specimen. As noted in the above compliance study, however, assumptions based on straight-through notch theory could not be used to determine Y^* values other than Y_m^*, because the agreement with the experimental results was poor.

The above assumptions regarding the compliance behaviour of the modified short bar allow for some preliminary fracture toughness determinations. Ultimately, however, confirmation of these assumptions for modified short bar specimens with or without the "outer" region is needed. Until a proper verification of the A_m value is performed, the K_{IcSB} values reported in this study cannot be taken as absolute values. Still, they do give some indication as to the toughness of these interfaces while also allowing for relative comparisons between groups.

4.4. K_{IcSB} and strain energy release rates

From theoretical analyses of interface fracture mechanics [38, 39], it has been inferred that the critical strain energy release rate, G_c, may be a more appropriate means of characterizing interface toughness because it essentially represents the energy required to create new surfaces. The more universal nature of G_c compared to the corresponding K_c value was illustrated by Melcholsky and Barker [30] in their examination of composite short bars in which one-half of the specimen was ceramic and the other metal. In their study, the toughness values measured for the interface depended on which material was chosen to have the standard half dimensions. Only the value $(K_{IcSB})^2/E_1$ ($= G_{Ic}$), where E_1 is the elastic modulus of the standard half, was invariant.

In the current study, K_{IcSB} has been used throughout to characterize interface toughness. From the previous section, it has been shown, however, that the two halves of the modified short bar are, to all intents and purposes, identical. Thus, in this case, K_{IcSB} appears to be an appropriate measure of interface toughness.

4.5. K_{IcSB} and mixed mode stress intensities

In this study, the interface toughness of these plasma spray-coated systems has been characterized using K_{IcSB}. However, from a review of fracture mechanics literature [39–43], it is apparent that a more complex situation potentially exists at this plasma-sprayed ceramic/metal substrate interface. Indeed, in preliminary observations, Colin *et al.* [21] detected Mode I and Mode II cracking at this interface using acoustic emission monitoring, with the Mode II cracking accounting for emissions with lower pulse count rates.

Several factors may contribute to more complex stress intensities at this metal/ceramic interface. Aside from the obvious differences in elastic properties of the materials on either side of the interface (which is the basis of the most complex stress intensity theory), there is also potentially significant shear (Mode II) loading arising from the thermal expansion mismatch between the plasma-sprayed ceramic and the metal substrate [38]. Complicating the situation further is the nonplanarity of these interfaces due to the necessary surface roughening of the substrate prior to coating deposition. Crack surface contact at these "undulations" can ultimately have an effect on the overall fracture resistance of the interface [43]. Whether these factors will significantly alter the interface toughness evaluations performed in this study cannot be readily discerned. It is apparent, however, that further studies of these plasma-sprayed ceramic/metal substrate interfaces need to expand upon this preliminary work, at least from a theoretical standpoint, to include these issues of complex stress intensities and potential mixed-mode fracture behaviour.

4.6. Choice of bonding agent

An important consideration in the assembly and testing of both the tensile and modified short-bar specimens was the choice of adhesive or bonding agent. Excessive adhesive penetration into the coating can alter the test data considerably; artificially high bond strength values can result, for example, from bonding between the adhesive and the underlying metal substrate, or the "filling" or reinforcing of defect structures such as pores (which can act as stress concentrators) and weak interlamellar bonding [11, 44, 45]. If the porosity or voids comprising the coating are of the "open" or interconnected variety, which may comprise upwards of 90% of the total porosity [46], the likelihood of this outcome is further heightened.

For this alumina study, A2 epoxy adhesive with activator W was chosen as the bonding agent because when compared to A12, a similar epoxy recommended by ASTM C633, A2/W possessed higher tensile strength properties with a higher viscosity. A2/W also did not undergo any shrinkage during curing. As added precautions to excessive adhesive penetration into the coating, Teflon tape (tensile specimens) or modelling clay (short-bar) was used around the coating edges of all specimens, and assembly and curing occurred with the coating facing down.

4.7. Controlling plasma-spraying parameters

Ideally, in a study attempting to characterize a particular system, one would like to be able to reproduce that system at will, or at least readily account for changes to that system. Several parameters are involved in the creation of well-adhering plasma-sprayed coatings [8]. Additionally, many of these parameters do not operate independently and are, in fact, functions of several parameters. Thus, unexpected changes in coating morphology or adherence cannot always be readily explained, particularly if care is not taken to monitor as many of the unassigned (i.e. "controllable") parameters as is possible. Even with the US alumina-coating studies, for which semi-automated control was available and the need for reproducibility emphasized, unanticipated though seemingly insignificant alterations in equipment design resulted in measurable changes in coating adhesion. Ultimately, then, before any characterization technique can be applied to these plasma-sprayed systems, one needs to fully appreciate the overall complexity of these systems and recognize the extent to which coating conditions can be controlled.

5. Conclusions

1. A modified short-bar test was developed to measure the fracture toughness of this plasma-sprayed ceramic/metal substrate interface. Preliminary evaluations of the alumina-coated Ti–6Al–4V systems revealed generally brittle behaviour at this interface. An interface toughness value of $1.84 \pm 0.20\ \mathrm{MPa\,m^{1/2}}$ was obtained for the primary alumina study group. This measurement was shown to be insensitive to the weakly bonded coating region incorporated into the specimen design partly as a "pre-cracking" mechanism.

2. Further refinement of this modified short-bar technique, taking into account experimental compliance behaviour and potential complex or mixed-mode stress intensities, is needed to confirm these preliminary toughness values. Improvements in the monitoring of mouth opening displacement are also required. Still, this technique offers a potentially more sensitive means of evaluating the mechanical integrity of these metal/ceramic interfaces than is possible with the tensile test.

3. In this study, a lower tensile adhesive bond strength than has been previously reported for this system was obtained. Non-optimized spraying parameters in this study and, perhaps more importantly, adhesive penetration effects in the earlier studies might have accounted for some of this difference.

4. Minor alterations in plasma-spraying parameters resulted in some significant changes in the mechanical integrity of the metal/ceramic interface. Diligent control of these parameters is thus necessary for a meaningful evaluation of these interfaces.

Acknowledgements

We thank the Plasma Technology Research Centre, University of Sherbrooke, and Jay-Em Ceramics, Inc., Brampton, Ontario, for providing the plasma-sprayed alumina coatings, and the Civil Engineering Materials Group, University of Toronto, for the mercury porosimetry data. We are also grateful to Mr Dave Abdulla for his technical assistance. This study was funded by the Natural Sciences and Engineering Research Council of Canada and the Ontario Centre for Materials Research.

References

1. I. KVERNES, M. ESPELAND and O. NORHOLM, *Scand. J. Metall.* **17** (1988), 8.
2. K. T. SCOTT, in "Ceramic Surfaces and Surface Treatments" (British Ceramic Society, Shelton, 1984) p. 195.
3. P. CHAGNON and P. FAUCHAIS, *Ceram. Int.* **10** (4) (1984) 119.
4. R. C. TUCKER, in "Deposition Technologies for Films and Coatings", edited by R. F. Bunshah (Noyes, Park Ridge, 1982) p. 454.
5. C. C. BERNDT and R. McPHERSON, *Aust. Weld. Res.* **6** (1979) 75.
6. P. OSTOJIC and C. C. BERNDT, *Surf. Coat. Technol.* **34** (1) (1988) 43.
7. C. C. BERNDT, in "Advances in Fracture Research", Vol. 4, edited by S. R. Valluri, B. M. R. Taplin, P. Rama Rao, J. F. Knott and R. Dubey (Pergamon Press, Oxford, 1984) p. 2553.
8. D. A. GERDEMAN and N. L. HECHT, "Arc Plasma Technology in Materials Science" (Springer-Verlag, New York, 1972) p. 9.
9. W. DIEM, G. ELSSNER, T. SUGA and G. PETZOW, in "Adhesive Joints: Formation, Characteristics, and Testing", edited by K. L. Mittal (Plenum Press, New York, 1984) p. 871.
10. D. S. RICKERBY, *Surf. Coat. Technol.* **36** (1988) 541.
11. H. S. INGHAM, in "Adhesion Measurement of Thin Films, Thick Films, and Bulk Coatings", ASTM STP 640, edited by K. L. Mittal (American Society for Testing and Materials, Philadelphia, PA, 1978) p. 285.
12. E. LOPEZ, F. BELTZUNG and G. ZAMBELLI, *J. Mater. Sci. Lett.* **8** (1989) 346.
13. General specification, ASTM D3359 (American Society for Testing and Materials, Philadelphia, PA, 1983).
14. M. J. FILIAGGI, N. A. COOMBS and R. M. PILLIAR, *Mater. Res. Soc. Symp. Proc.* **153** (1989) 377.
15. C. C. BERNDT, in "Ultrastructure Processing of Ceramics, Glasses, and Composites", edited by L. L. Heich and D. R. Ulrich (Wiley, New York, 1984) p. 524.
16. C. C. BERNDT and R. McPHERSON, in "Surfaces and Interfaces in Ceramic and Ceramic-Metal Systems", edited by J. Pask and A. Evans (Plenum Press, New York, 1981) p. 619.
17. C. C. BERNDT, in "Advances in Fracture Research", Vol. 4, edited by S. R. Valluri, B. M. R. Taplin, P. Rama Rao, J. F. Knott and R. Dubey (Pergamon Press, Oxford, 1984) p. 2545.
18. G. N. HEINTZE and R. McPHERSON, *Surf. Coat. Technol.* **34** (1988) 15.
19. *Idem, ibid.* **36** (1988) 125.
20. P. OSTOJIC and R. McPHERSON, *J. Amer. Ceram. Soc.* **71** (1988) 891.
21. C. COLIN, M. BOUSSUGE, D. VALENTIN and G. DESPLANCHES, *J. Mater. Sci.* **23** (1988) 2121.
22. M. K. FERBER and S. D. BROWN, in "Fracture Mechanics of Ceramics", Vol. 6, edited by R. C. Bradt, A. G. Evans, D. P. H. Hasselman and F. F. Lange (Plenum Press, New York, 1983) p. 523.
23. M. K. FERBER, PhD thesis, University of Illinois at Urbana-Champaign (1981).
24. J. C. NEWMAN, in "Chevron-notched specimens: Testing and Stress Analysis", ASTM STP 855, edited by J. H. Underwood, S. W. Freiman and F. I. Baratta (American Society for Testing and Materials, Philadelphia, PA, 1984) p. 5.
25. D. H. SHERMAN, *Metals Handbook* **8** (1985) 468.
26. K. R. BROWN, *ASTM Standard News* **16** (11) (1988) 66.
27. D. MUNZ, R. T. BUBSEY and J. E. SRAWLEY, *Int. J. Fract.* **16** (1980) 359.
28. L. M. BARKER, *Engng. Fract. Mech.* **9** (1977) 361.
29. *Idem, Int. J. Fract.* **15** (1979) 515.
30. J. J. MELCHOLSKY and L. M. BARKER, in "Chevron-notched Specimens: Testing and Stress Analysis", ASTM STP 855, edited by J. H. Underwood, S. W. Freiman and F. I. Baratta (American Society for Testing and Materials, Philadelphia, PA, 1984) p. 324.
31. L. M. BARKER, *Eng. Fract. Mech.* **17** (1983) 289.
32. S. SAFAI and H. HERMAN, in "Advances in Surface Coating Technology", edited by J. C. Anderson (The Welding Institute, Cambridge, 1978) p. 1.
33. D. J. VARACELLE, *Mater. Res. Soc. Symp. Proc.* **121** (1988) 541.
34. V. WILMS and H. HERMAN, *Thin Solid Films* **39** (1976) 251.
35. S. D. BROWN, J. L. DRUMMOND, M. K. FERBER, D. P. REED and M. R. SIMON, in "Mechanical Properties of Biomaterials", edited by G. W. Hastings and D. F. Williams (Wiley, Chichester, 1980) p. 249.
36. J. E. RANDALL and D. DOWSON, *Engng. Med.* **13** (2) (1984) 67.
37. F. GITZHOFER, personal communication, University of Sherbrooke, Quebec (1989).
38. P. O. CHARREYRON, N. J. BYLINA and J. G. HANNOOSH, in "Fracture Mechanics of Ceramics", Vol. 8, edited by R. C. Bradt, A. G. Evans, D. P. H. Hasselman and F. F. Lange (Plenum Press, New York, 1986) p. 225.
39. T. SUGA and G. ELSSNER, *J. de Phys.* **46** (C4) (1985) 657.
40. J. R. RICE, *J. Appl. Mech.* **55** (1988) 98.
41. H. T. CORTEN, in "Fracture: An Advanced Treatise", Vol. VII, edited by H. Liebowitz (Academic Press, New York, 1972) p. 675.
42. F. ERDOGAN, *J. Appl. Mech.* **32** (1965) 403.
43. A. G. EVANS and J. W. HUTCHINSON, *Acta Metall.* **37** (1989) 909.
44. E. BARDAL, P. MOLDE, and T. G. EGGEN, *Brit. Corros. J.* **8** (1973) 15.
45. F. J. HERMANEK, *Weld. J.* **57** (11) (1978) 31.
46. P. BOCH, P. FAUCHAIS, D. LOMBARD, B. ROGEAUX and M. VARDELLE, in "Science and Technology of Zirconia II", edited by N. Claussen, M. Ruhle and A. H. Heuer (American Ceramic Society, Columbus, 1984) p. 488.

Received 11 September 1990
and accepted 21 January 1991